

Retraction

Retracted: DOA Estimation of an Enhanced Generalized Nested Array with Increased Degrees of Freedom and Reduced Mutual Coupling

International Journal of Antennas and Propagation

Received 19 December 2023; Accepted 19 December 2023; Published 20 December 2023

Copyright © 2023 International Journal of Antennas and Propagation. This is an open access article distributed under the Creative Commons Attribution License, which permits unrestricted use, distribution, and reproduction in any medium, provided the original work is properly cited.

This article has been retracted by Hindawi following an investigation undertaken by the publisher [1]. This investigation has uncovered evidence of one or more of the following indicators of systematic manipulation of the publication process:

- (1) Discrepancies in scope
- (2) Discrepancies in the description of the research reported
- (3) Discrepancies between the availability of data and the research described
- (4) Inappropriate citations
- (5) Incoherent, meaningless and/or irrelevant content included in the article
- (6) Manipulated or compromised peer review

The presence of these indicators undermines our confidence in the integrity of the article's content and we cannot, therefore, vouch for its reliability. Please note that this notice is intended solely to alert readers that the content of this article is unreliable. We have not investigated whether authors were aware of or involved in the systematic manipulation of the publication process.

Wiley and Hindawi regrets that the usual quality checks did not identify these issues before publication and have since put additional measures in place to safeguard research integrity.

We wish to credit our own Research Integrity and Research Publishing teams and anonymous and named external researchers and research integrity experts for contributing to this investigation.

The corresponding author, as the representative of all authors, has been given the opportunity to register their agreement or disagreement to this retraction. We have kept a record of any response received.

References

- [1] Y. Zhang, G. Hu, J. Shi, H. Zhou, C. Zhan, and F. Zhao, "DOA Estimation of an Enhanced Generalized Nested Array with Increased Degrees of Freedom and Reduced Mutual Coupling," *International Journal of Antennas and Propagation*, vol. 2021, Article ID 7233651, 13 pages, 2021.

Research Article

DOA Estimation of an Enhanced Generalized Nested Array with Increased Degrees of Freedom and Reduced Mutual Coupling

Yule Zhang ,^{1,2} **Guoping Hu** ,² **Junpeng Shi** ,³ **Hao Zhou** ,² **Chenghong Zhan** ,^{1,2} and **Fangzheng Zhao** ,^{1,2}

¹Graduate College, Air Force Engineering University, Xi'an 710051, China

²Air and Missile Defense College, Air Force Engineering University, Xi'an 710051, China

³College of Electronic Countermeasure, National University of Defense Technology, Hefei 230037, China

Correspondence should be addressed to Guoping Hu; guoping_hu6068@163.com

Received 8 May 2021; Accepted 25 September 2021; Published 14 October 2021

Academic Editor: Liangtian Wan

Copyright © 2021 Yule Zhang et al. This is an open access article distributed under the Creative Commons Attribution License, which permits unrestricted use, distribution, and reproduction in any medium, provided the original work is properly cited.

Aiming at low degrees of freedom (DOF) and high mutual coupling (MC) of the existing sparse arrays, an enhanced generalized nested array (EGNA) is proposed in this paper. Specifically, the proposed array adds a single antenna on the basis of generalized nested array (GNA), and the difference of coprime factors is employed as the spacing between the second subarray and the additional antenna. Then, the values of the coprime factors are analyzed in detail, which indicates that Yang-NA can be explained as a special case. Compared with the majority of the existing sparse arrays, EGNA not only has the closed-form expressions of the physical antenna locations, consecutive lags, and unique lags, but also significantly increases DOF and reduces MC. In view of the above advantages, EGNA can obtain superior performance in direction of arrival (DOA) estimation. Numerical simulation results verify the rationality and superiority of the proposed nested array.

1. Introduction

A basic technology of array signal processing is the direction of arrival (DOA) estimation, which is also one of the essential research tasks in the fields of communications, radar, sonar, and electronic countermeasures in the past decades and future [1–4]. The conventional DOA estimation generally considers uniform linear array (ULA) in theoretical research and engineering applications, whereas the antenna spacing is no more than half wavelength. Hence, the following problems arise. On one hand, when the signal frequency is too high, the arrangement of physical antennas is difficult to be realized due to the smaller interelement spacing, and large mutual coupling (MC) [5–7] will occur. On the other hand, high resolution means larger array aperture and more physical antennas, which will further increase the cost and complexity of the system.

Over the years, sparse arrays (e.g., the minimum redundancy array (MRA) [8–10], nested array (NA) [11], and coprime array (CPA) [12–14]) have attracted a lot of interest

due to the concept of difference coarray (DCA) [15, 16] and significant degrees of freedom (DOF). Furthermore, compared with ULA, the larger interelement spacing of sparse arrays can further expand the virtual aperture and effectively suppress the MC of antennas, thereby increasing the number of detectable sources and angular resolution and improving the estimation accuracy.

BouDaher et al. [17] analyzed the influence of MC on DOA estimation, proving that MRA is least affected by MC, but it is difficult to obtain the effective closed-form expressions of DOF. CPA is alternately composed of two sparse uniform linear arrays with coprime interelement spacing, which has low MC as a result of the large interelement spacing, whereas the staggered distribution of the two subarrays leads to a smaller array aperture and lower DOF. By contrast, NA has definite physical antenna positions and closed-form expressions of DOF and can obtain more DOF. However, the interelement spacing of the first-level subarray of NA is still half wavelength, which causes serious MC. To this end, several modified configurations

have been derived. Zhao et al. [18] and Iizuka et al. [19] adjusted the interelement spacing of NA and obtained optimized nested configurations with higher DOF. Yang et al. [20] established an improved nested array by introducing an additional antenna, which has higher DOF than NA, and its DCA is a virtual uniform linear array without holes. Simultaneously, the increase of the subarrays interelement spacing alleviates MC between the antennas. Liu et al. [21, 22] constructed a super nested array (SNA) by designing a specific system program to determine the location of antennas, which has less MC due to fewer adjacent antennas. Chen et al. [23] proposed a loosely distributed nested array (LoDiNA) that generate greater DOF with higher robustness against MC. Shi et al. [24] flexibly adjusted the interelement spacing of NA and obtained a generalized nested array (GNA) with lower MC, but it does not enhance DOF. Nevertheless, these modifications only consider one of the DOF and MC, which limits DOA estimation performance.

With the intention of ulteriorly increasing DOF and reducing MC at the same time, we propose an enhanced generalized nested array (EGNA) in this paper. In short, EGNA exploits two coprime factors to increase the interelement spacing of two-level nested array and takes the difference of these two coprime integers as the spacing between the second subarray and the additional antenna. The closed-form expressions of the consecutive lags, and DOF are deduced. Then, according to different coprime factors, the DCA of EGNA is analyzed from the maximizing consecutive lags and maximizing unique lags. In general, EGNA has the following superiorities.

- (a) By introducing the coprime factors, EGNA can flexibly adjust the interelement spacing according to actual needs. In addition, Yang-NA [20] can be considered as a special case of EGNA.
- (b) EGNA has the same DOF as Yang-NA, but with less MC, especially for the larger coprime factors.
- (c) Both EGNA and GNA [24] have less MC, but DOF of EGNA is higher than that of NA, ENA [18], Iizuka-NA [19], SNA, CPA, LoDiNA, and GNA.

The remainder of this paper is organized as follows. Several preliminaries are briefly reviewed in Section 2. Section 3 describes the signal model with MC. Section 4 elaborates on EGNA and compares it with the existing linear array. Section 5 evaluates the DOA performances of EGNA based on the simulation experiments. The conclusion is presented in Section 6.

1.1. Notations. In this paper, we use boldfaced italic uppercase and boldfaced italic lowercase letters to denote

matrices and vectors, respectively. $(\cdot)^T$, $(\cdot)^H$, and $(\cdot)^*$ represent a matrix/vector transpose operator, the conjugate transpose operator, and the complex conjugate operator, respectively. \odot and \otimes stand for the Khatri–Rao product and Kronecker product. $|\cdot|$ represents absolute value. $\|\cdot\|_0$, $\|\cdot\|_1$, and $\|\cdot\|_2$ denote the l_0 -norm, l_1 -norm, and l_2 -norm, respectively. $\text{diag}(\cdot)$ is the diagonal matrix operator. $E[\cdot]$ and $\text{vec}(\cdot)$ represent the expectation and the vectorization operator, respectively. \mathbb{Z}^+ denotes the set of positive integers.

2. Preliminaries

In order to facilitate the discussion of our proposed EGNA, we will briefly review some preliminary knowledge of DCA, DOF, weight value, Yang-NA, and GNA in this section.

2.1. DCA, DOF, and Weight Value

Definition 1 (difference coarray). Let us consider two sets of integers $P = \{p_1, p_2, \dots, p_m\}$ and $D = \{d_1, d_2, \dots, d_n\}$.

Define the self-difference coarray S_s as

$$S_s = \{p_i - p_j | 1 \leq i, j \leq m\} \cup \{d_i - d_j | 1 \leq i, j \leq n\}. \quad (1)$$

Define the cross-difference coarray S_c as

$$S_c = \{\pm(p_i - d_j) | 1 \leq i \leq m, 1 \leq j \leq n\}. \quad (2)$$

The difference coarray S is the union set of the self-difference coarray S_s and the cross-difference coarray S_c .

$$S = S_s \cup S_c. \quad (3)$$

Definition 2 (degrees of freedom). In (3), if duplicate elements are allowed in the difference coarray S , the total number of disparate elements is defined as degrees of freedom.

Definition 3 (weight value). The weight value $\omega(\cdot)$ refers to the number of virtual array elements appearing in the DCA.

2.2. Yang-NA. As depicted in Figure 1, Yang-NA [20] is composed of two ULAs and an additional antenna, where the first level has M_1 antennas, and the interelement spacing is d ; the second level has M_2 antennas, and the interelement spacing is $(M_1 + 2)d$; and the spacing between the second level and the additional antenna is $(M_1 + 1)d$. Herein, $d = \lambda/2$ is the unit interelement spacing and λ denotes the signal wavelength.

Then, the antenna positions set can be given as

$$P_{\text{Yang-NA}} = \{0, 1, \dots, M_1 - 1, M_1, M_1 + (M_1 + 2), \dots, M_1 + (M_2 - 1)(M_1 + 2), M_1 + (M_2 - 1)(M_1 + 2) + M_1 + 1\}. \quad (4)$$

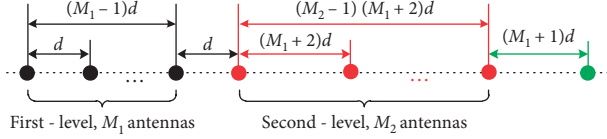


FIGURE 1: Yang-NA configuration.

Yang-NA has the closed-form expressions of the antenna locations and DOF, and a larger DCA without holes can be provided than NA..

2.3. GNA. The original intention of GNA [24] is to alleviate mutual coupling. As presented in Figure 2, the interelement spacing is two coprime integers.

Then, the antenna positions set can be expressed as

$$P_{GNA} = \{0, \alpha, \dots, \alpha M_1, \alpha M_1 + \beta, \dots, \alpha M_1 + \beta(M_2 - 1)\}. \quad (5)$$

GNA has the closed-form expressions for the unique lags, which greatly reduces the mutual coupling while maintaining the DOF as NA.

3. Signal Model with Mutual Coupling

Assume that there are K far-field narrowband uncorrelated target incidents on a sparse array with G antennas from $\theta = \{\theta_k = k = 1, 2, \dots, K\}$. Then, the signal with mutual coupling can be modeled as

$$\mathbf{x}(t) = \mathbf{C}\mathbf{A}\mathbf{s}(t) + \mathbf{n}(t), \quad (6)$$

where $\mathbf{A} = [\mathbf{a}(\theta_1), \mathbf{a}(\theta_2), \dots, \mathbf{a}(\theta_K)]$ is the steering matrix and $\mathbf{a}(\theta_k) = [1, e^{-j2\pi d_2 d \sin \theta_k / \lambda}, \dots, e^{-j2\pi d_G d \sin \theta_k / \lambda}]^T$ is the steering vector of the k -th source. d_i is the spacing between the i -th and the first antenna, where $d_1 = 0$. $\mathbf{s}(t) = [s_1(t), s_2(t), \dots, s_K(t)]^T$ denotes the target vector and $s_k(t)$ is the baseband waveform of the k -th source. $\mathbf{n}(t)$ represents the independent and identically distributed white Gaussian noise vector. \mathbf{C} is the mutual coupling matrix introduced in [21], which can be approximated as a Toeplitz matrix with B-banded symmetry [25].

$$\mathbf{C}_{ij} = \begin{cases} c_{|d_i-d_j|}, & |d_i - d_j| \leq B, \\ 0, & |d_i - d_j| > B, \end{cases} \quad (7)$$

where \mathbf{C}_{ij} is the element in the i -th row and the j -th column of \mathbf{C} , and $1 = c_0 > c_1 > \dots > |c_B| > |c_{B+1}| = 0$.

For the convenience of measuring the influence of mutual coupling, it can be defined as

$$\Omega = \frac{\|\mathbf{C} - \text{diag}(\mathbf{C})\|_2}{\|\mathbf{C}\|_2}, \quad (8)$$

where $[\text{diag}(\mathbf{C})]_{ij} = \mathbf{C}_{ij}\delta_{ij}$, and δ_{ij} is the Dirichlet function. It can be seen from (8) that the smaller the Ω is, the weaker the mutual coupling effect will be.

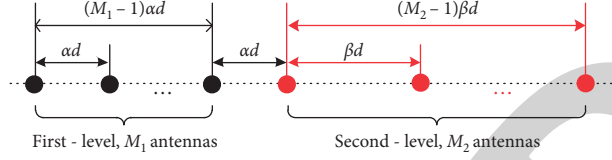


FIGURE 2: GNA configuration.

Afterwards, the signal covariance matrix under the condition of mutual coupling can be calculated as

$$\mathbf{R} = E[\mathbf{x}(t)\mathbf{x}^H(t)] = \mathbf{C}\mathbf{A}^H\mathbf{C}^H + \sigma_n^2\mathbf{I}_G, \quad (9)$$

where $\mathbf{R}_s = E[\mathbf{s}(t)\mathbf{s}^H(t)] = \text{diag}[\sigma_1^2, \sigma_2^2, \dots, \sigma_K^2]$ represents the source covariance matrix. σ_k^2 is the signal power of the k -th source. σ_n^2 is the noise power. \mathbf{I}_G is the $G \times G$ -dimensional identity matrix.

In practical application, \mathbf{R} can usually be estimated by

$$\widehat{\mathbf{R}} = \frac{1}{L} \sum_{t=1}^L \mathbf{x}(t)\mathbf{x}^H(t), \quad (10)$$

where L denotes the number of snapshots and $\widehat{\mathbf{R}}$ is an estimate of \mathbf{R} .

Next, the observing vector \mathbf{r} can be obtained by vectorizing the covariance matrix \mathbf{R} .

$$\begin{aligned} \mathbf{r} = \text{vec}(\mathbf{R}) &= ((\mathbf{C}\mathbf{A})^* \odot (\mathbf{C}\mathbf{A}))\mathbf{p} + \sigma_n^2 \text{vec}(\mathbf{I}_G) \\ &= \mathbf{C}_0(\mathbf{A}^* \odot \mathbf{A})\mathbf{p} + \sigma_n^2 \text{vec}(\mathbf{I}_G), \end{aligned} \quad (11)$$

where $\mathbf{C}_0 = \mathbf{C}^* \otimes \mathbf{C}$. $\mathbf{p} = [\sigma_1^2, \sigma_2^2, \dots, \sigma_K^2]^T$.

$$\mathbf{A}^* \odot \mathbf{A} = [\mathbf{a}^*(\theta_1) \otimes \mathbf{a}(\theta_1), \mathbf{a}^*(\theta_2) \otimes \mathbf{a}(\theta_2), \dots, \mathbf{a}^*(\theta_K) \otimes \mathbf{a}(\theta_K)] \quad (12)$$

is the virtual steering array matrix of single snapshot measurement \mathbf{r} .

Therefore, the virtual array positions of matrix $\mathbf{A}^* \odot \mathbf{A}$ are composed of the DCA of the physical antenna positions.

4. Enhanced Generalized Nested Array

GNA exploits two coprime extension factors to increase the interelement spacing of the nested array to reduce mutual coupling, while Yang-NA adds an additional antenna on the basis of NA and sets different interelement spacing for the subarray to improve the DOF. Therefore, we can introduce the idea of generalization into Yang-NA and establish an enhanced generalized nested array to achieve joint optimization of degrees of freedom and mutual coupling, as shown in Figure 3. EGNA can be obtained by introducing the interelement spacing coprime extension factors into the basic configuration of Yang-NA, where the interelement spacing of the first subarray is αd , and the number of antennas is M_1 ; the second subarray has M_2 antennas with the interelement spacing of βd ; and the spacing between the second subarray and the additional antenna is $(\beta - \alpha)d$. α and β are two coprime integers.

Then, the positions of antennas can be given as

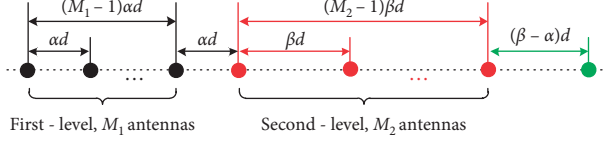


FIGURE 3: Enhanced generalized nested array.

$$P_{EGNA} = \{0, \alpha, \dots, \alpha M_1, \alpha M_1 + \beta, \alpha M_1 + 2\beta, \dots, \alpha M_1 + \beta(M_2 - 1), \alpha(M_1 - 1) + \beta M_2\}. \quad (13)$$

Subsequently, combining Figure 3 and (13), we can get the following definition.

Definition 4. The DCA of EGNA can be defined as

$$\begin{aligned} S_{EGNA} &= S_{EGNA}^+ \cup S_{EGNA}^-, \\ S_{EGNA}^+ &= \{x_n - x_{\tilde{n}} \mid x_n \geq x_{\tilde{n}}, x_n, x_{\tilde{n}} \in P_{EGNA}\}, \end{aligned} \quad (14)$$

where S_{EGNA}^+ and S_{EGNA}^- denote the positive elements set and negative elements set of S_{EGNA} , respectively.

Combined with Definition 4, the characteristics of S_{EGNA} can be derived as the following lemma.

Lemma 1. The configuration of EGNA and the corresponding DCA set are presented in Figure 3 and (14), respectively. Then, S_{EGNA} has the following characteristics:

- (a) When $1 \leq \alpha \leq M_2$, $2 \leq \beta \leq M_1 + 2$, and $\alpha < \beta$, the range of consecutive lags in S_{EGNA}^+ can be expressed as $[(\alpha - 1)(\beta - 1) - \alpha, \alpha(M_1 - 1) + \beta M_2 - (\alpha - 1)(\beta - 1) + \alpha]$.
- (b) When $1 \leq \alpha \leq M_2$, $2 \leq \beta \leq M_1 + 2$, and $\alpha < \beta$, the DOF of the set S_{EGNA} is equal to $2g + 1$, where $g = \alpha(M_1 - 1) + \beta M_2 - (\alpha - 1)(\beta - 1) + 2\alpha - 2$.

Proof

- (a) From Definition 4, the DCA S_{EGNA}^+ includes the self-difference coarray S_{s-EG}^+ and the cross-difference coarray S_{c-EG}^+ . Then, S_{EGNA}^+ can be expressed as

$$\begin{aligned} S_{EGNA}^+ &= S_{s-EG}^+ \cup S_{c-EG}^+, \\ S_{s-EG}^+ &= \{\alpha m_1 \mid m_1 \in [0, M_1 - 1]\} \cup \{\beta m_2 \mid m_2 \in [0, M_2 - 1]\}, \\ S_{c-EG}^+ &= \{\alpha m_1 + \beta m_2 \mid m_1 \in [0, M_1 - 1], m_2 \in [0, M_2]\}. \end{aligned} \quad (15)$$

Due to $S_{s-EG}^+ \subset S_{c-EG}^+$, (15) can be restated as

$$\begin{aligned} S_{EGNA}^+ &= S_{s-EG}^+ \cup S_{c-EG}^+ \\ &= \{\alpha m_1 + \beta m_2 \mid m_1 \in [0, M_1 - 1], m_2 \in [0, M_2]\}. \end{aligned} \quad (16)$$

According to Definition 4 and (16), we need to prove that there are $m_1 \in [0, M_1 - 1]$ and $m_2 \in [0, M_2]$ so that $s = \alpha m_1 + \beta m_2$ contains all the consecutive lags from $(\alpha - 1)(\beta - 1) - \alpha$ to $\alpha(M_1 - 1) + \beta M_2 - (\alpha - 1)(\beta - 1) + \alpha$,

where $1 \leq \alpha \leq M_2$, $2 \leq \beta \leq M_1 + 2$, $\alpha < \beta$, α and β are two coprime integers.

Firstly, we can rewrite the condition $0 \leq m_1 \leq M_1 - 1$ as

$$0 \leq \alpha m_1 \leq \alpha(M_1 - 1). \quad (17)$$

Secondly, by substituting $\alpha m_1 = s - \beta m_2$ and $(\alpha - 1)(\beta - 1) - \alpha \leq s \leq \alpha(M_1 - 1) + \beta M_2 - (\alpha - 1)(\beta - 1) + \alpha$ into (17), we can obtain

$$\begin{aligned} \alpha(\beta - M_1 - 2) + \alpha - \beta + 1 &\leq \beta m_2 \\ &\leq \alpha(M_1 + 2 - \beta) + \beta M_2 - \alpha + \beta - 1. \end{aligned} \quad (18)$$

On account of $2 \leq \beta \leq M_1 + 2$, we have $\beta - M_1 - 2 \leq 0$, $M_1 + 2 - \beta \geq 0$. Hence, (18) can be represented as

$$\begin{aligned} \alpha - \beta + 1 &\leq \beta m_2 \leq \beta M_2 - (\alpha - \beta + 1) \\ \Rightarrow \frac{(\alpha - \beta + 1)}{\beta} &\leq m_2 \leq M_2 - \frac{(\alpha - \beta + 1)}{\beta}. \end{aligned} \quad (19)$$

Since $\alpha < \beta$, $\beta \geq 2$, we can obtain

$$\frac{(\alpha - \beta + 1)}{\beta} < \frac{1}{\beta} < 1. \quad (20)$$

Thus, $0 \leq m_2 \leq M_2$.

- (b) We take the positive integer set S_{EGNA}^+ as an example; i.e., it is necessary to prove that there exist $g + 1$ virtual array elements in S_{EGNA}^+ , where $g = \alpha(M_1 - 1) + \beta M_2 - (\alpha - 1)(\beta - 1) + 2\alpha - 2$.

The maximum value of S_{EGNA}^+ can be obtained from (16):

$$g_{\max} = \alpha(M_1 - 1) + \beta M_2. \quad (21)$$

The distribution of virtual array elements in S_{EGNA}^+ is shown in Figure 4. The virtual array elements are composed of three parts, namely, discrete part 1, consecutive part, and discrete part 2.

From (21), it can be seen that the number of virtual array elements g_2 of discrete part 2 satisfies

$$\begin{aligned} 0 \leq g_2 &\leq (g_{\max} + \alpha) - (\alpha(M_1 - 1) + \beta M_2 - (\alpha - 1)(\beta - 1) + \alpha) \\ &\Rightarrow 0 \leq g_2 \leq (\alpha - 1)(\beta - 1). \end{aligned} \quad (22)$$

In order to determine the size of g_2 , the geometric distribution of α and β is established in Figure 5. Since D_1 and D_2 are symmetric, the two parts contain the same

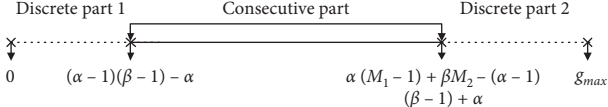
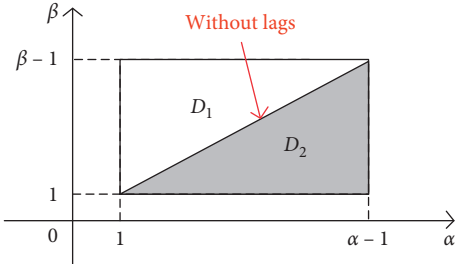


FIGURE 4: Schematic diagram of virtual array element distribution.

FIGURE 5: Geometric distribution of α and β .

number of virtual array elements. In addition, α and β are two coprime integers, so there are no virtual array elements on the diagonal. Thus, the total number of virtual array elements is $g_2 = (\alpha - 1)(\beta - 1)/2 - 1$.

Similarly, the number of virtual array elements g_1 contained in discrete part 1 also satisfies

$$g_1 = (\alpha - 1)(\beta - 1)/2 - 1. \quad (23)$$

As a result, the total number of S_{EGNA}^+ satisfies

$$\begin{aligned} g &= [\alpha(M_1 - 1) + \beta M_2 - (\alpha - 1)(\beta - 1) + \alpha] \\ &\quad - [(\alpha - 1)(\beta - 1) + \alpha] + g_1 + g_2 = \alpha(M_1 - 1) \\ &\quad + \beta M_2 - (\alpha - 1)(\beta - 1) + 2\alpha - 2. \end{aligned} \quad (24)$$

EGNA and GNA are generalizations of Yang-NA and NA, respectively. To better illustrate their differences, we will provide two types of special cases to understand the lemma, namely, maximizing consecutive lags and maximizing unique lags. \square

$$2(M_1 - 1) + \beta M_2 - (\beta - 3) - (\beta - 3) + 1 = 2G + (\beta - 2)M_2 + 3 - 2\beta =$$

4.1. Maximizing Consecutive Lags. It can be known from (23) that the number of discrete virtual array elements in S_{EGNA}^+ is equal to $(\alpha - 1)(\beta - 1) - 2$. Consequently, only when $\alpha = 1$, $\beta \in [2, M_1 + 2]$ or $\alpha = 2$, $\beta = 3$, there are no holes in the DCA of EGNA; i.e., the number of unique lags is the same as the consecutive lags. Next, we will detailedly analyze the above two cases, in which GNA is provided for comparison.

(a) Case 1 ($\alpha = 1$, $\beta \in [2, M_1 + 2]$).

The ranges of the consecutive lags in S_{EGNA}^+ and S_{GNA}^+ [24] are $[(\alpha - 1)(\beta - 1) - \alpha, \alpha(M_1 - 1) + \beta M_2 - (\alpha - 1)(\beta - 1) + \alpha]$ and $[(\alpha - 1)(\beta - 1), \alpha M_1 + \beta M_2 - \alpha\beta + \alpha - 1]$, respectively. Therefore, when $\alpha = 1$, $\beta \in [2, M_1 + 2]$, we can get that the range of the consecutive lags in S_{EGNA}^+ is $[-1, M_1 + \beta M_2] \Rightarrow [0, M_1 + \beta M_2]$. Besides, when $\alpha = 1$, $\beta \in [1, M_1 + 1]$, the range of the consecutive lags in S_{GNA}^+ is $[0, M_1 + \beta(M_2 - 1)]$. In addition, the total numbers of antennas for EGNA and GNA are $M_1 + M_2 + 1$ and $M_1 + M_2$, respectively, so we have $S_{EGNA}^+ \geq S_{GNA}^+$.

Particularly, we can know from (4) and (13) that when $\alpha = 1$, $\beta = M_1 + 2$, we have $\beta - \alpha = M_1 + 1$. At the moment, EGNA is exactly equal to Yang-NA, whose DCA is kept as a ULA without holes. Hence, Yang-NA can be identified as a special case of EGNA. Similarly, for GNA, if $\alpha = 1$, $\beta = M_1 + 1$, the configuration of GNA is the same as NA. Moreover, it is proved that Yang-NA has a larger array aperture and better DOA estimation performance than NA [20].

(b) Case 2 ($\alpha = 2$, $\beta = 2k + 1$ ($k \in \mathbb{Z}^+$)).

It can be obviously known that when $\alpha = 2$, $\beta = 2k + 1$ ($k \in \mathbb{Z}^+$), the ranges of the consecutive lags in S_{EGNA}^+ and S_{GNA}^+ are $[\beta - 3, 2(M_1 - 1) + \beta M_2 - (\beta - 3)]$ and $[\beta - 1, 2M_1 + \beta M_2 - 2\beta + 1]$, respectively.

The number of consecutive lags in S_{EGNA}^+ is

$$2(M_1 - 1) + \beta M_2 - (\beta - 3) - (\beta - 3) + 1 = 2G + (\beta - 2)M_2 + 3 - 2\beta = \begin{cases} \frac{[(\beta + 2)G + 6 - 4\beta]}{2} & G \text{ is Even } \left(M_2 = \frac{G}{2} \right) \\ \frac{[(\beta + 2)G + 4 - 3\beta]}{2} & G \text{ is Odd } \left(M_2 = \frac{(G + 1)}{2} \right) \end{cases}. \quad (25)$$

The number of consecutive lags in S_{GNA}^+ is

$$2M_1 + \beta M_2 - 2\beta + 1 - (\beta - 1) + 1 = 2G + (\beta - 2)M_2 + 3 - 3\beta = \begin{cases} \frac{[(\beta + 2)G + 6 - 6\beta]}{2} & G \text{ is Even } \left(M_2 = \frac{G}{2} \right) \\ \frac{[(\beta + 2)G + 4 - 5\beta]}{2} & G \text{ is Odd } \left(M_2 = \frac{(G + 1)}{2} \right) \end{cases}. \quad (26)$$

$$2M_1 + \beta M_2 - 2\beta + 1 - (\beta - 1) + 1 = 2G + (\beta - 2)M_2 + 3 - 3\beta =$$

Particularly, for EGNA, if $\alpha = 2$, $\beta = 3$, the discrete virtual holes will not appear in the DCA. However, for GNA, when $\alpha = 2$, $\beta = 3$, there are 2 holes in the S_{GNA}^+ [24]; i.e., the number of unique lags will exceed that of consecutive lags.

Based on the above analysis, we can conclude that whether the number of antennas is even or odd, the range of consecutive lags in S_{EGNA}^+ is larger than or equal to that of S_{GNA}^+ .

4.2. Maximizing Unique Lags. In case of $\alpha \neq 1$ or $\alpha \neq 2$, $\beta \neq 3$, there are discrete virtual holes in the DCA of EGNA, whereas, for GNA, there exist discrete virtual holes as long as $\alpha \neq 1$ or $\beta \neq 1$. The holes will increase with the increase of α and β , resulting in fewer consecutive lags. Nevertheless, we can greatly reduce the MC by flexibly changing α and β .

According to (8), MC is mainly determined by the inter-element spacing. Specifically, when $\alpha > B$, $\beta > B$, and $\beta - \alpha > B$, $\Omega = 0$; when $\alpha \leq B$, $\beta \leq B$ or $\beta - \alpha \leq B$, $\Omega > 0$. Supposing $M_1 > B$, $M_2 > B$, and $G = M_1 + M_2 + 1$, the joint optimization model of DOF and MC can be established as follows:

$$\begin{aligned} \max_{\alpha, \beta} g &= \alpha(M_1 - 1) + \beta M_2 - (\alpha - 1)(\beta - 1) + 2\alpha - 2 \\ \text{s.t. } &B < \alpha \leq M_2, \\ &B < \beta \leq M_1 + 2, \\ &\beta - \alpha > B, G = M_1 + M_2 + 1. \end{aligned} \quad (27)$$

condition of GNA. We can see that when the number of antennas is small, the optimization condition of $\beta - \alpha > B$ cannot be satisfied. Once the number of antennas is large, it is not necessary to consider. (4) Compared with CPA, EGNA does not need the prerequisite that the number of two subarrays is coprime, but only the inter-element spacing is coprime. Thus, the array arrangement will be more flexible. (5) From the perspective of configuration, the number of antennas of EGNA is less restrictive than SNA and LoDiNA. EGNA only requires $M_1 \geq 1$, $M_2 \geq 2$, while SNA and LoDiNA needs to meet $M_1 \geq 4$, $M_2 \geq 3$ and $M_1 \geq 3$, $M_2 \geq 3$, respectively. This means that SNA and LoDiNA are ineffective when the number of antennas is less than 7 and 5, respectively, while EGNA can obtain a valid configuration when the number of antennas exceeds 4.

Proof. Firstly, we calculate the partial derivative of the variable g with respect to the parameters α and β .

$$\begin{aligned} \frac{\partial g}{\partial \alpha} &= M_1 + 2 - \beta \geq 0, \\ \frac{\partial g}{\partial \beta} &= M_2 + 1 - \alpha \geq 0. \end{aligned} \quad (28)$$

Therefore, the variable g is a monotonically increasing function. Therefore, when α or β reaches the maximum value, the variable g reaches the maximum. To determine its exact range, the variable g can be reexpressed.

$$\begin{aligned} g &= \alpha(M_1 - 1) + \beta M_2 - (\alpha - 1)(\beta - 1) + 2\alpha - 2 \\ &= \alpha(M_1 + 2 - \beta) + \beta(M_2 + 1) - 3 \\ &= \beta(M_2 + 1 - \alpha) + \alpha(M_1 + 2) - 3. \end{aligned} \quad (29)$$

From (29), we can see that when $\beta = M_1 + 2$, $\alpha \in (B, M_2]$, the variable g can take the maximum value; i.e., $g = M_1 M_2 + M_1 + 2M_2 - 1$. Then, according to the Arithmetic Mean–Geometric Mean (AM–GM) inequalities, the antenna configuration results are shown in Table 1.

To facilitate comparison, we first summarize the closed-form expressions of DOF of various array geometries (namely, NA, ENA, Iizuka-NA, Yang-NA, CPA, LoDiNA, GNA, and EGNA) in Table 2.

Compared with maximizing consecutive lags, maximizing unique lags can obtain a larger DOF and effective array aperture. In addition, a more flexible α makes the configuration of EGNA more realistic. It can be also found that when α takes a larger value, the interelement spacing of the first subarray becomes larger, which greatly reduces MC. However, when the maximizing consecutive lags is achieved, the smaller α causes no significant improvement in the MC of the first subarray. \square

4.2.1. Remarks. After the joint optimization of DOF and MC, the excellent characteristics of EGNA can be listed as follows: (1) We can see that EGNA retains the original advantages of Yang-NA, which has the simple closed-form expressions with physical antennas and DOF. (2) In case of $\alpha \in [1, M_2]$, $\beta = M_1 + 2$, EGNA has the same DOF as Yang-NA and has more DOF than NA, ENA, Iizuka-NA, SNA, CPA, LoDiNA, and GNA. (3) In terms of MC, both GNA and EGNA exploit two coprime extension factors to expand the interelement spacing, so their MC is much lower than the existing sparse arrays. Moreover, $\beta - \alpha$ is employed as the spacing between the second level and the single antenna of EGNA to mitigate MC, which is distinct from the optimization condition of GNA. We can see that when the number of antennas is small, the optimization condition of $\beta - \alpha > B$ cannot be satisfied. Once the number of antennas is large, it is not necessary to consider. (4) Compared with CPA, EGNA does not need the prerequisite that the number of two subarrays is coprime, but only the inter-element spacing is coprime. Thus, the array arrangement will be more flexible. (5) From the perspective of configuration, the number of antennas of EGNA is less restrictive than SNA and LoDiNA. EGNA only requires $M_1 \geq 1$, $M_2 \geq 2$, while SNA and LoDiNA needs to meet $M_1 \geq 4$, $M_2 \geq 3$ and $M_1 \geq 3$, $M_2 \geq 3$, respectively. This means that SNA and LoDiNA are ineffective when the number of antennas is less than 7 and 5, respectively, while EGNA can obtain a valid configuration when the number of antennas exceeds 4.

In order to have a more explicit understanding of antenna and virtual element positions for different array geometries, Figure 6 depicts the physical antenna distribution and virtual array element expansion of various array structures, where the number of physical antennas is 10. It can be clearly seen that the DOF of NA, ENA, Iizuka-NA, Yang-NA, SNA, CPA, LoDiNA, GNA, and EGNA are 59, 61, 61, 67, 59, 39, 61, 59, and 67, respectively. The DOF of EGNA is the same as Yang-NA and higher than the other arrays, while EGNA can overcome the influence of MC by flexibly adjusting the interelement spacing. Moreover, the ranges of the consecutive lags of GNA and EGNA are [20, 29] and [15, 30], respectively. Both GNA and EGNA adopt the generalized idea, but EGNA can obtain more consecutive lags than those of GNA.

TABLE 1: Optimal configuration structure for EGNA.

G	Optimal M_1, M_2	Optimal α, β	g	g_{\max}
Even	$M_1 = G/2 - 1, M_2 = G/2$	$B < \alpha \leq M_2, \beta = M_1 + 2$	$M_1 M_2 + M_1 + 2M_2 - 1$	$(G^2 + 4G - 8)/4$
Odd	$M_1 = (G - 1)/2 - 1, M_2 = (G + 1)/2$	$B < \alpha < M_2, \beta = M_1 + 2$	$M_1 M_2 + M_1 + 2M_2 - 1$	$(G^2 + 4G - 9)/4$

TABLE 2: Comparison of DOF for different arrays.

Total number of antennas	NA	ENA	Iizuka-NA	Yang-NA	CPA	LoDiNA	GNA	EGNA
8	39	41	41	45	27	41	39	45
9	49	49	51	55	29	51	49	55
12	83	85	85	93	53	85	83	93
14	111	113	113	123	69	113	111	123
17	161	161	163	175	93	163	161	175
19	199	199	201	215	117	201	199	215
DOF	G is even G is odd	$(G^2 + 2G - 2)/2$ $(G^2 + 2G - 1)/2$	$(G^2 + 2G + 2)/2$ $(G^2 + 2G - 1)/2$	$(G^2 + 2G + 2)/2$ $(G^2 + 2G + 3)/2$	$(G^2 + 4G - 6)/2$ $(G^2 + 4G - 7)/2$	$M_1 M_2 + M_1 + M_2 - 2$	$(G^2 + 2G + 2)/2$ $(G^2 + 2G + 3)/2$	$(G^2 + 2G - 2)/2$ $(G^2 + 2G - 1)/2$

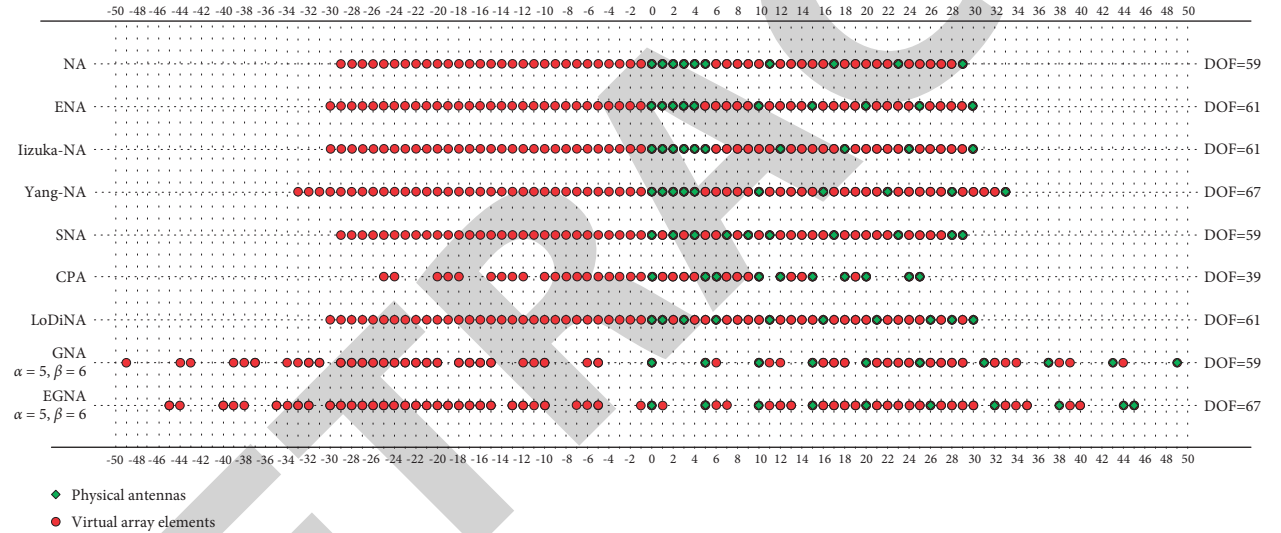


FIGURE 6: Schematic diagram of antenna distribution and virtual array element expansion of various arrays (the number of physical antennas is 10).

Then, we can utilize a spatial signal recovery method based on Lasso optimization proposed in [26] for DOA estimation, specifically as follows:

$$\hat{q}_0 = \arg \min \left[\frac{1}{2} \|\mathbf{r} - \tilde{\mathbf{B}} \mathbf{q}_0\|_2 + \lambda_t \|\mathbf{q}_0\|_1 \right], \quad (30)$$

where l_1 -norm denotes a spatial constraint, l_2 -norm represents the least square cost function, and λ_t is a penalty parameter used to balance the estimation of the least square error of nonzero, which is set as 2.15 based on experience. The above objective function can be optimized using the CVX toolkit.

5. Simulation Experiments

In this section, we employ the CS algorithm for DOA estimation and several numerical experiments to evaluate the performance of the proposed nested array, where NA, ENA, Iizuka-NA, Yang-NA, SNA, CPA, LoDiNA, and GNA are provided for comparison.

5.1. Experiment Setting. Suppose that the total number of physical antennas is 16; i.e., $M_1 = 7, M_2 = 8$. The parameters in the mutual coupling matrix \mathbf{C} are set as $c_0 = 1, c_1 = 0.5e^{j\pi/4}, c_2 = 0.5e^{j0.7\pi}/2, c_3 = 0.5e^{j0.7\pi}/3, B = 3$ [24].

TABLE 3: Comparison of MC for different geometries.

Array structure	Physical antenna positions	MC
NA	{0, 1, 2, 3, 4, 5, 6, 7, 8, 17, 26, 35, 44, 53, 62, 71}	0.6987
ENA	{0, 1, 2, 3, 4, 5, 6, 7, 16, 24, 32, 40, 48, 56, 64, 72}	0.6857
Iizuka-NA	{0, 1, 2, 3, 4, 5, 6, 7, 8, 18, 27, 36, 45, 54, 63, 72}	0.6987
Yang-NA	{0, 1, 2, 3, 4, 5, 6, 7, 16, 25, 34, 43, 52, 61, 70, 78}	0.6857
SNA	{0, 2, 4, 5, 7, 10, 12, 15, 17, 26, 35, 44, 53, 62, 70, 71}	0.4876
CPA	{0, 8, 9, 16, 18, 24, 27, 32, 36, 40, 45, 48, 54, 56, 63, 64}	0.3574
LoDiNA	{0, 4, 8, 12, 16, 20, 24, 28, 32, 41, 50, 59, 68, 77, 86, 95}	0.4855
GNA	{0, 4, 8, 12, 16, 20, 24, 28, 32, 41, 50, 59, 68, 77, 86, 95}	0
EGNA	{0, 4, 8, 12, 16, 20, 24, 28, 37, 46, 55, 64, 73, 82, 91, 96}	0

According to the optimization results, we assume $\alpha = 4$, $\beta = 9$.

5.2. Degrees of Freedom and Mutual Coupling. Table 3 shows a comparison of antenna positions and MC between different array geometries at 16 antennas. It can be seen from Figure 7 and Table 3 that NA and Iizuka-NA have the largest MC due to the densely distributed subarrays and CPA has the lowest DOF owing to the coprime relationship between the number of antennas. Though ENA, Yang-NA, and LoDiNA have higher DOF than NA, the dense subarrays still have higher MC. Even though SNA, CPA, LoDiNA, and GNA have lower MC than NA, their DOF are limited. Compared with the above sparse array geometries, EGNA can increase DOF while reducing MC by improving the interelement spacing.

Figure 7 plots the relationship between the number of DOF and physical antennas for different array structures. We can clearly see that EGNA and Yang-NA can obtain more DOF than that of CPA and the gap between them increases with the number of physical antennas, while the DOF curves of other array structures slowly change between these two sets of curves.

Figure 8 depicts the relationship between the positions and weight values of the DCA for different array structures. It can be seen that NA, ENA, Iizuka-NA, Yang-NA, SNA, and LoDiNA can all obtain continuous virtual array elements, while CPA, GNA, and EGNA have discrete virtual array elements. ENA, Iizuka-NA, Yang-NA, SNA, and LoDiNA retain the original advantages of NA, and their DCA are ULA without holes. Since the interelement spacing and the number of subarrays of CPA are both coprime integers, the DCA has discrete holes. The DCA of GNA and EGNA are not ULAs without holes due to the coprime of the interelement spacing. It should be pointed out that EGNA and GNA have a larger interelement spacing and fewer virtual array elements near the zero position ($\omega(1) = \omega(-1) = \omega(2) = \omega(-2) = \omega(3) = \omega(-3) = 0$). Thus the mutual coupling is the smallest. NA and Iizuka-NA have more virtual array elements near the zero position and larger weight value ($\omega(-1) = \omega(1) = 8, \omega(-2) = \omega(2) = 7, \omega(-3) = \omega(3) = 6$) than other array structures, so the mutual coupling is the largest.

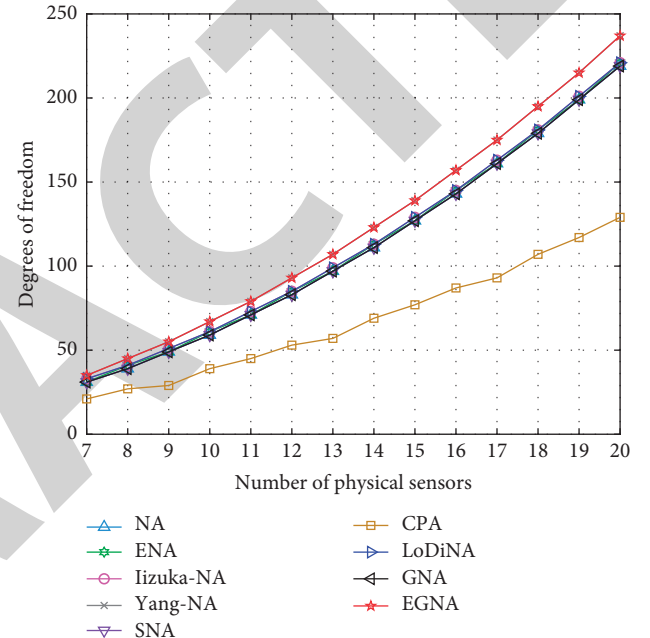


FIGURE 7: DOF versus the number of physical antennas.

5.3. CS Spectrum. To further illustrate the estimation performance of the proposed nested array, Figure 9 shows the CS spectrum of various array configurations, where $\text{SNR} = 0 \text{ dB}$ and the number of snapshots L is set as 100. 21 far-field narrowband uncorrelated targets are located at $[-30^\circ: 3^\circ: 30^\circ]$, and the red dash-dotted line represents the true angle direction. The search range is -35° to 35° , and the searching grid is 0.1° . As can be seen from Figure 9, NA, ENA, Iizuka-NA, and Yang-NA have the weakest estimation performance due to the highest MC. SNA, CPA, and LoDiNA can estimate 17, 20, and 16 targets, respectively, while GNA and EGNA can identify all targets. Although GNA has the same DOF as NA, lower MC makes its CS spectrum estimation performance better than that of other array structures. Moreover, EGNA has a better CS spectrum than GNA. Therefore, EGNA can obtain better DOA estimation performance than existing sparse arrays by joint optimizing DOF and MC.

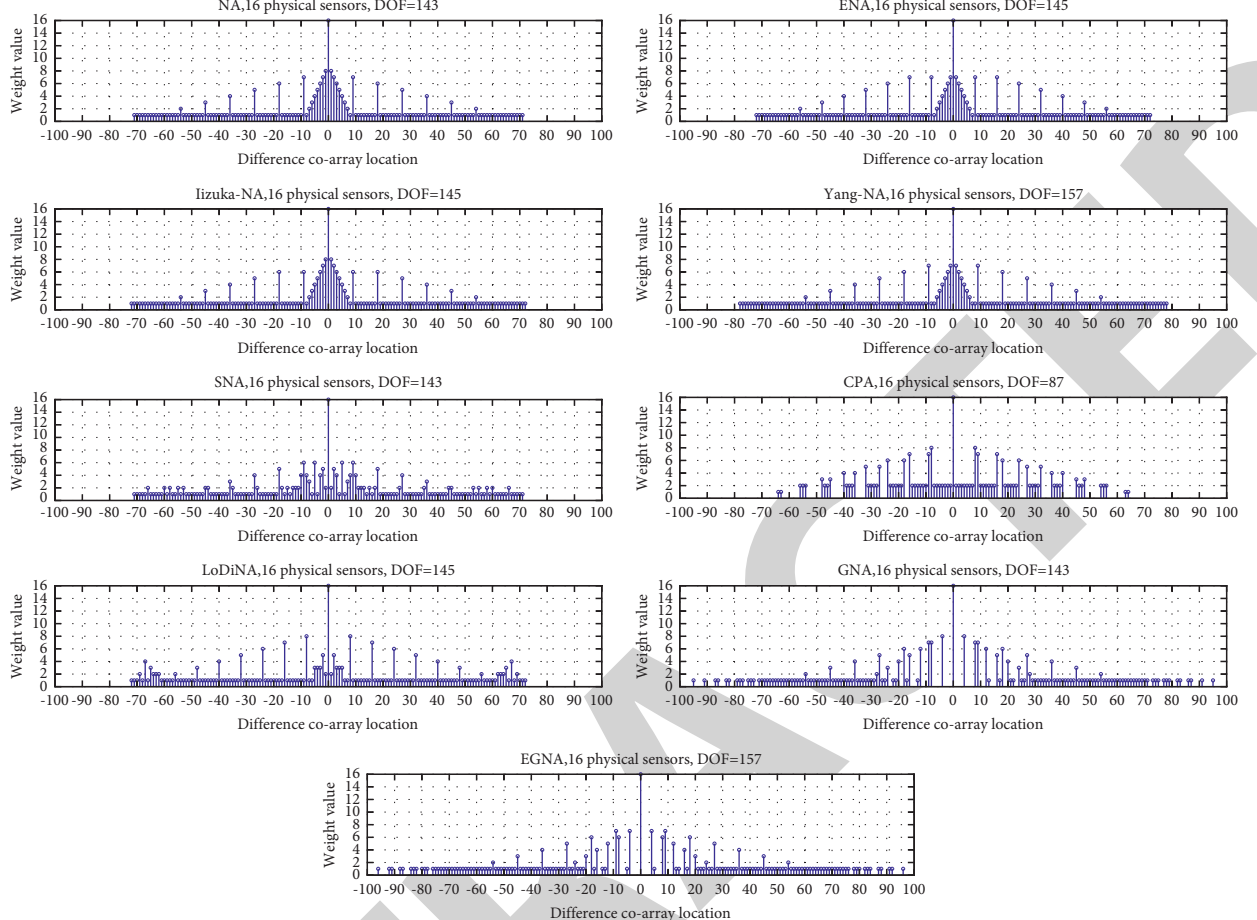


FIGURE 8: Comparison of difference coarray location for different array structures.

5.4. Root Mean Square Error (RMSE). In this part, RMSE of DOA estimation for EGNA and other arrays are compared via Monte Carlo experiments. Figure 10 describes the relationship between RMSE of DOA estimation and SNR, where the number of snapshots L is 100. Figure 11 shows the relationship between RMSE and the number of snapshots, where $\text{SNR} = 0 \text{ dB}$. Assume that the sources are located at $[5^\circ, 8^\circ, 11^\circ]$. The search range is 0° to 15° , and the searching grid is 0.01° . The RMSE of DOA estimation can be calculated as

$$\text{RMSE} = \sqrt{\frac{1}{TK} \sum_{i=1}^T \sum_{k=1}^K \left(\hat{\theta}_k^i - \theta_k \right)^2}, \quad (31)$$

where $T = 200$ is the total number of Monte Carlo experiments, θ_k denotes the true DOA, and $\hat{\theta}_k^i$ denotes the estimated DOA in the i -th experiments.

As can be seen from Figures 10 and 11, the estimation performance of each array geometry is gradually improved with the increase of SNR and the number of

snapshots. In particular, EGNA has the optimal estimation performance by increasing DOF and reducing MC of antennas. Furthermore, although the DOF of CPA is lower, it has better estimation performance than NA owing to the smaller MC. Therefore, reducing MC is of great significance for improving array estimation performance.

5.5. Resolution Performance. Figure 12 depicts the close targets resolution performance of different array geometries. Here, the definition of resolution can be found in [27]. Suppose two nearby targets are distributed in 5° and 6° , where $\text{SNR} = -10 \text{ dB}$ and the number of snapshots is 50. The search range is $[1^\circ, 10^\circ]$, and the searching grid is 0.01° . It can be seen from Figure 12 that NA, ENA, Iizuka-NA, Yang-NA, SNA, and CPA can only estimate one target, and the CS spectrums obviously deviate from the true angle. LoDiNA, GNA, and EGNA can distinguish the above two targets, whereas EGNA has a higher precision CS spectrum than LoDiNA and GNA.

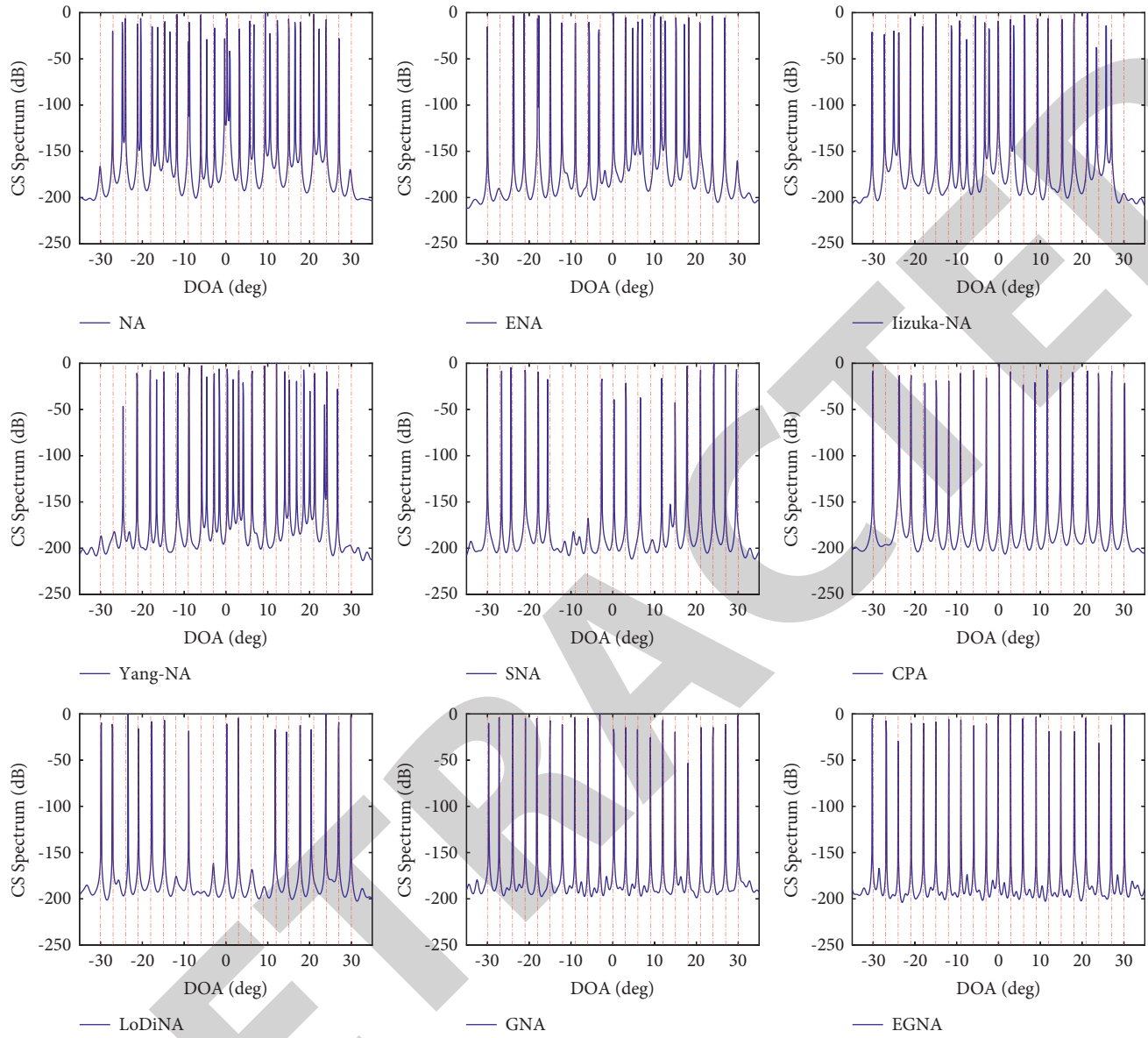


FIGURE 9: Comparison of CS spectrum for different array configurations.

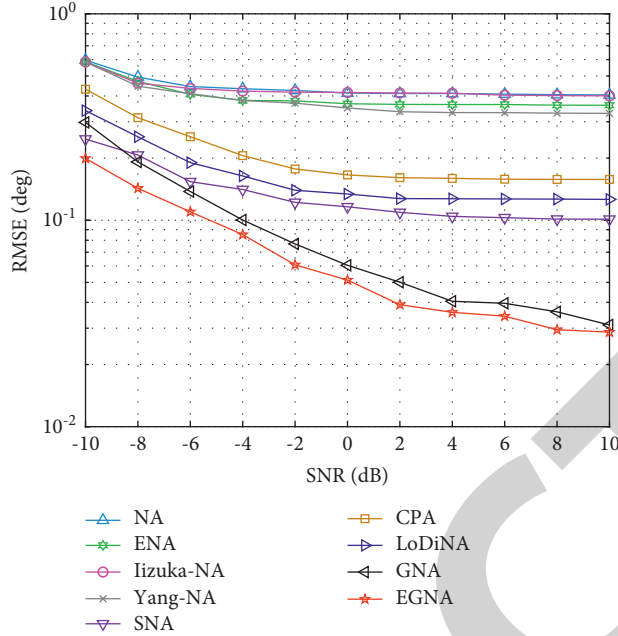


FIGURE 10: RMSE versus SNR for different array geometries.

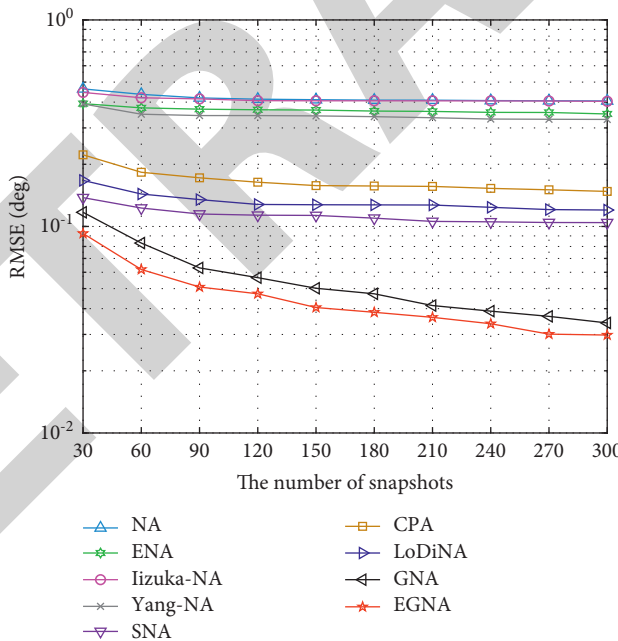


FIGURE 11: RMSE versus the number of snapshots for different array geometries.

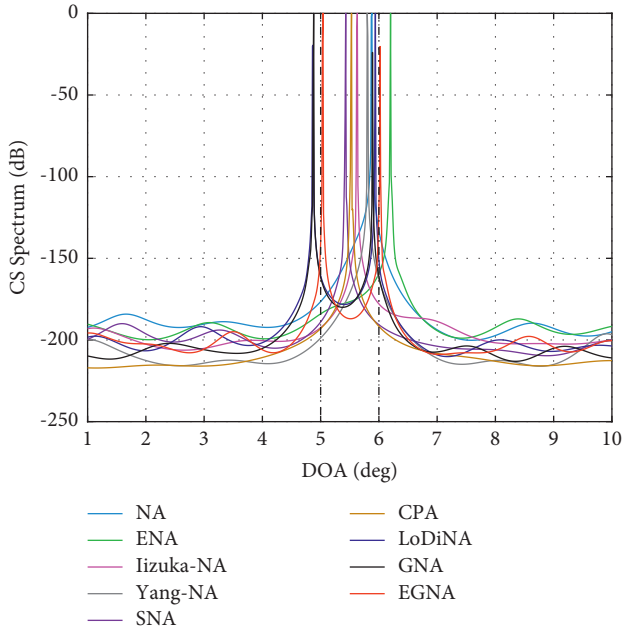


FIGURE 12: CS spectrum of two nearby targets for different array geometries.

6. Conclusion

In this paper, we have proposed an enhanced generalized nested array, and Yang-NA can be considered as a special case. By adjusting the interelement spacing, EGNA can achieve joint optimization of degrees of freedom and mutual coupling, which has explicit physical antenna positions and closed-form expressions. It was proved that EGNA can obtain the same degrees of freedom as Yang-NA and higher degrees of freedom than GNA, but with lower mutual coupling. Simulation experiments show that the more degrees of freedom and less mutual coupling lead to significant advantages over the existing sparse array structures in terms of spatial spectrum and DOA estimation accuracy.

Data Availability

The data supporting the conclusion of the study are shown in the research paper.

Conflicts of Interest

The authors declare that there are no conflicts of interest regarding the publication of this paper.

Acknowledgments

The authors would like to appreciate Mingming Zhu and Shijie Yue of Air and Missile Defense College, Air Force Engineering University, for their theoretical guidance and assistance with the experiments. This work was supported by the National Natural Science Foundation of China under Grant no. 61871395.

References

- [1] H. Abeida and J. P. Delmas, "Robustness of subspace-based algorithms with respect to the distribution of the noise: application to DOA estimation," *Signal Processing*, vol. 164, pp. 313–319, 2019.
- [2] F. Wen, J. Shi, and Z. Zhang, "Closed-form estimation algorithm for EMVS-MIMO radar with arbitrary sensor geometry," *Signal Processing*, vol. 186, no. 8, 2021.
- [3] P. Chen, Z. Cao, Z. Chen, and X. Wang, "Off-Grid DOA estimation using sparse bayesian learning in MIMO radar with unknown mutual coupling," *IEEE Transactions on Signal Processing*, vol. 67, no. 1, pp. 208–220, 2019.
- [4] J. Shi, F. Wen, and T. Liu, "Nested MIMO radar: coarrays, tensor modeling and angle estimation," *IEEE Transactions on Aerospace and Electronic Systems*, vol. 57, no. 1, pp. 573–585, 2021.
- [5] Z. Zhongfu Ye, J. Jisheng Dai, X. Xu Xu, and X. Xiaopei Wu, "DOA estimation for uniform linear array with mutual coupling," *IEEE Transactions on Aerospace and Electronic Systems*, vol. 45, no. 1, pp. 280–288, 2009.
- [6] S. Cai, J. Zhang, G. Wang, H. Zhu, and K. K. Wong, "Subspace methods for self-calibration of ULAs with unknown mutual coupling: a false-peak analysis," *Signal Processing*, vol. 174, 2020.
- [7] X. Zhang, T. Jiang, Y. Li, and Y. Zakharov, "A novel block sparse reconstruction method for DOA estimation with unknown mutual coupling," *IEEE Communications Letters*, vol. 23, no. 10, pp. 1845–1848, 2019.
- [8] A. Moffet, "Minimum-redundancy linear arrays," *IEEE Transactions on Antennas and Propagation*, vol. 16, no. 2, pp. 172–175, 1968.
- [9] D. A. Linebarger, I. H. Sudborough, and I. G. Tollis, "Difference bases and sparse sensor arrays," *IEEE Transactions on Information Theory*, vol. 39, no. 3, pp. 716–721, 1993.
- [10] C. S. Ruf, "Numerical annealing of low-redundancy linear arrays," *IEEE Transactions on Antennas and Propagation*, vol. 41, no. 1, pp. 85–90, 1993.
- [11] P. Pal and P. P. Vaidyanathan, "Nested arrays: a novel approach to array processing with enhanced degrees of freedom," *IEEE Transactions on Signal Processing*, vol. 58, no. 8, pp. 4167–4181, 2010.
- [12] P. P. Vaidyanathan and P. Pal, "Sparse sensing with Co-prime samplers and arrays," *IEEE Transactions on Signal Processing*, vol. 59, no. 2, pp. 573–586, 2011.
- [13] P. Pal and P. P. Vaidyanathan, "Coprime sampling and the MUSIC algorithm," in *Proceedings of the 14th IEEE DSP/SPE Workshop*, pp. 289–294, Sedona, AZ, USA, January 2011.
- [14] P. P. Vaidyanathan and P. Pal, "Sparse sensing with coprime arrays," in *Proceedings of the 44th Asilomar Conference Signals, System Computation*, pp. 1405–1409, Pacific Grove, CA, USA, November 2010.
- [15] W.-K. Ma, T.-H. Hsieh, and C.-Y. Chi, "DOA estimation of quasi-stationary signals with less sensors than sources and unknown spatial noise covariance: a khatri-rao subspace approach," *IEEE Transactions on Signal Processing*, vol. 58, no. 4, pp. 2168–2180, 2010.
- [16] Q. Shen, W. Cui, W. Liu, S. Wu, Y. D. Zhang, and M. G. Amin, "Underdetermined wideband DOA estimation of off-grid sources employing the difference co-array concept," *Signal Processing*, vol. 130, pp. 299–304, 2017.
- [17] E. BouDaher, F. Ahmad, M. G. Amin, and A. Hoofar, "Mutual coupling effect and compensation in non-uniform

- arrays for direction-of-arrival estimation," *Digital Signal Processing*, vol. 61, no. 1, pp. 3–14, 2017.
- [18] P. Zhao, G. Hu, Z. Qu, and L. Wang, "Enhanced nested array configuration with hole-free co-array and increasing degrees of freedom for DOA estimation," *IEEE Communications Letters*, vol. 23, no. 12, pp. 2224–2228, 2019.
- [19] Y. Izuka and K. Ichige, "Extension of nested array for large aperture and high degree of freedom," *IEICE Communications Express*, vol. 6, no. 6, pp. 381–386, 2017.
- [20] M. Yang, L. Sun, X. Yuan, and B. Chen, "Improved nested array with hole-free DCA and more degrees of freedom," *Electronics Letters*, vol. 52, no. 25, pp. 2068–2070, 2016.
- [21] C.-L. Liu and P. P. Vaidyanathan, "Super nested arrays: linear sparse arrays with reduced mutual coupling-Part I: Fundamentals," *IEEE Transactions on Signal Processing*, vol. 64, no. 15, pp. 3997–4012, 2016.
- [22] C.-L. Liu and P. P. Vaidyanathan, "Super nested arrays: linear sparse arrays with reduced mutual coupling-Part II: high-order extensions," *IEEE Transactions on Signal Processing*, vol. 64, no. 16, pp. 4203–4217, 2016.
- [23] M. Chen, L. Gan, and W. Wang, "A new sparse linear array with three-level nested structure," in *Proceedings of the 2019 Sensor Signal Processing for Defense Conference (SSPD)*, Brighton, UK, May, 2019.
- [24] J. Shi, G. Hu, X. Zhang, and H. Zhou, "Generalized nested array: optimization for degrees of freedom and mutual coupling," *IEEE Communications Letters*, vol. 22, no. 6, pp. 1208–1211, 2018.
- [25] C. Zhou, Y. Gu, S. He, and Z. Shi, "A robust and efficient algorithm for coprime array adaptive beamforming," *IEEE Transactions on Vehicular Technology*, vol. 67, no. 2, pp. 1099–1112, 2018.
- [26] R. Tibshirani, "Regression shrinkage and selection via the LASSO," *Journal of the Royal Statistical Society: Series B*, vol. 58, no. 1, pp. 267–288, 1996.
- [27] Y. Zhang, G. Hu, H. Zhou, M. Zhu, and F. Zhang, "DOA estimation of a novel generalized nested MIMO radar with high degrees of freedom and hole-free difference coarray," *Mathematical Problems in Engineering*, vol. 2021, Article ID 6622154, 9 pages, 2021.